RESEARCH ARTICLE

Performance of a laboratory von Hámos type x-ray spectrometer in x-ray absorption spectroscopy study on 3d group metals

Rafał Fanselow[1] | Michał Sobstel[2] | Wojciech Błachucki[1] | Jakub Szlachetko[3]

[1]Institute of Nuclear Physics Polish Academy of Sciences, Krakow, Poland

[2]Faculty of Biochemistry, Biophysics and Biotechnology, Jagiellonian University, Krakow, Poland

[3]SOLARIS National Synchrotron Radiation Centre, Jagiellonian University, Krakow, Poland

Correspondence
Jakub Szlachetko, National Synchrotron Radiation Centre SOLARIS, Jagiellonian University, Krakow, Poland.
Email: jakub.szlachetko@uj.edu.pl

Funding information
National Science Centre (Poland)

Abstract

With the recent progress regarding the development of x-ray instrumentation, compact x-ray spectrometers are becoming more and more popular as they allow x-ray absorption spectroscopy (XAS) and x-ray emission spectroscopy (XES) studies at the research institutes laboratories. Such setups provide a cost-effective tool for routine sample characterization with unlimited access and are of great utility in feasibility studies preceding the experiments at synchrotrons and x-ray free-electron lasers (XFELs). Herein, we present the operation and capabilities of the von Hámos type x-ray spectrometer in x-ray absorption spectra measurement for various 3d metal elements. Results allowed us to establish the photon counting performance of the setup, demonstrating a possible range of applications of the in-house x-ray spectroscopy apparatus.

KEYWORDS
lab-based x-ray spectrometer, von Hámos x-ray spectrometer, x-ray absorption spectroscopy

1 | INTRODUCTION

X-ray absorption spectroscopy (XAS) is a widely recognized analytical technique frequently applied by scientists to determine the electronic structure of various systems.[1] The penetrative nature of x-rays, in combination with the element-specificity of x-ray spectroscopy, allows bulk-sensitive examination of samples with loose restrictions regarding their form and environment. Thus, XAS is commonly employed in the fields of chemistry,[2] material engineering,[3] biology,[4] medicine,[5] environmental science[6] and many others for the characterization of bulk solids, powders, nanomaterials, colloids, liquids, and gases.[7,8]

Until recently, XAS experiments were performed almost exclusively using synchrotron sources.[9] These highly specialized, large-scale facilities produce very intense, monochromatic beam that, combined with well-developed detection systems, allow the acquisition of high-quality data, often within minutes of the measurement. For these reasons, synchrotrons became an irreplaceable tool for performing groundbreaking experiments that push the boundaries of science. However, such advanced facilities are very expensive therefore, the number of available beamlines worldwide is not sufficient to fulfill the demand of the scientific society. Access to synchrotron beamtime is limited and granted based on the proposal evaluation, which takes a lot of time to complete. Only a small percentage of applications are accepted, and the time allocated for performing a given experiment usually does not exceed a couple of

days. In addition, transferring samples to large-scale facilities, often located hundreds of kilometers from the home institution, is a logistic challenge, especially when specimens of interest require specific storage conditions due to their fragility or toxicity to the environment. These factors narrow the applications of XAS at synchrotrons primarily to the highest-priority queries.

Contrary to XAS, most scientific techniques, like x-ray diffraction or UV–VIS spectroscopy, are available for scientists not only at a cutting-edge level (synchrotrons or advanced laser facilities) but predominantly at a laboratory scale for routine day-to-day measurements. In-house equipment plays a very important role in most scientific projects as it guarantees constant access to a given method and thus allows long-term studies like the evaluation of synthetic procedures and systematic characterization of materials. Moreover, lab-based apparatus can also serve educational purposes, giving students an opportunity to familiarize themselves with its operation and possible utilization in their future research. The same benefits would apply to laboratory-scale x-ray spectrometers. Although examples of custom-made lab-based XAS setups were reported throughout the 20th century,[10–12] such devices never got adopted by broader scientific society, primarily due to long acquisition times and the complexity of certain technical aspects. However, the recent development of new compact instrumentation enabled researchers to resurrect the concept of in-house XAS setups. Indeed, during the last decade, the XAS community experienced the birth of so-called modern laboratory x-ray spectrometers.[8,9] These cost-effective systems allow ground-state characterization of concentrated samples with near-synchrotron quality under a few hours of measurement. Various pioneering lab-based spectrometers with the examples of their applications were presented by groups from Fribourg,[13] Seattle,[14] Budapest,[15] Berlin,[16] Helsinki,[17] and Warsaw[18] among others.

Some authors (W.B. and J.S.) also recognize the importance of laboratory setups for their daily use as a didactic tool for teaching young researchers. This aspect was particularly important in the laboratory led by the Professor Jean-Claude Dousse at the Department of Physics, the University of Fribourg (Switzerland), where we had a lifetime chance to conduct our Ph.D. studies. During the studies, we have learned that the laboratory x-ray systems are essential not only for scientific projects but, more importantly, very relevant for skills development of young researchers thanks to the opportunity of daily working with advanced instrumentation and developing own instrumental and methodological solutions. Professor Jean-Claude Dousse always said that the researcher has to "feel" the instrument in order to use it at best for research projects. We are following the message of the

Professor Jean-Claude Dousse, we have learned years ago, and nowadays, we are providing opportunities to young researchers to develop and discover new possibilities of x-ray spectroscopy systems, as presented here.

Since 2019, the laboratory XAS is also available at the Institute of Nuclear Physics of the Polish Academy of Sciences in Kraków. So far, our setup has been successfully utilized in studies of novel therapeutics[19] and nanomaterial suspensions[20] with more fascinating projects on the horizon. In this article, we wish to showcase the capabilities of our lab-based x-ray spectrometer by conducting a systematic study of 3d metals and establishing the photon counting performance limits of the setup paving the way toward wider popularity and applications of laboratory XAS. The presented setup will be extensively used for the characterization of metallic nanoparticles (NPs) and NPs-hybrid systems to track the electronic structure of in-house synthesized samples. This aspect is very relevant for laboratory experiments, as many plasmonic-hybrid materials are not stable and are difficult to be transported to synchrotron facilities for examination. For example, copper-based NPs are prone to immediate surface oxidation and only dedicated experimental protocols covering material synthesis and direct characterization at in-situ or almost in-situ conditions may be effectively used to map electronic states of the sample in the intact state.

2 | EXPERIMENTAL

Our setup is a slight modification of the one described in Ref. [18] and is depicted in Figure 1a,b in form of a schematic drawing and a photograph taken in the laboratory. It was designed in the von Hámos geometry. In this configuration x-ray beam transmitted through the sample falls on a cylindrically bent crystal that diffracts photons in one direction, according to the Braggs′ law, at the same time focusing them on the second axis. This allows the acquisition of the entire XAS spectrum without moving any part of the setup. The x-rays are produced by XOS X-beam Superflux PF x-ray Tube with a Mo anode with integrated focusing optics, which provides around $100 \times 100 \ \mu m^2$ spot on the sample placed in the beam focal point, which is 20 mm away from the optics′ exit. The crystals used in the presented study were cylindrically bent, segmented Si(440) or Si(400),[21] depending on the examined specimen, both with the radius curvature of 25 cm. The signal was registered by the Andor Newton DO920P camera equipped with a front-illuminated charge-coupled device (CCD) sensor of 1024×256 pixels, each with the size of 26 μm. The built-in thermoelectric system allows cooling the CCD sensor down to $-70°C$.
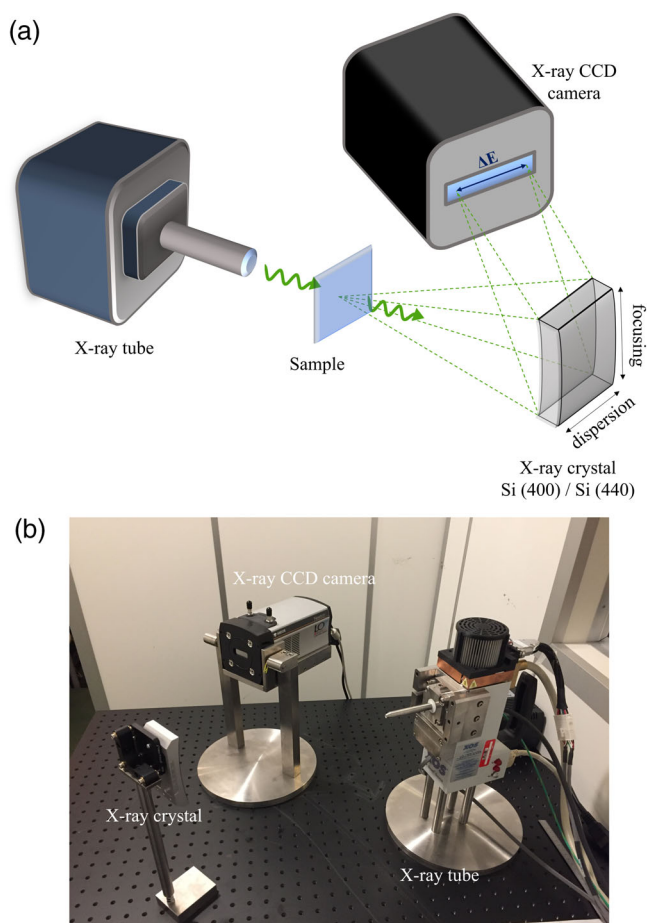
FIGURE 1 Lab-based setup for XAS studies: (a) schematical drawing, (b) photograph of the setup taken in the laboratory. [Colour figure can be viewed at wileyonlinelibrary.com]

The spectrometer resolving power was estimated to be at the level of $1–2 \times 10^{-4}$.[18] Noteworthily, the presented setup could be rearranged for x-ray emission spectroscopy (XES) studies providing information on the occupied electron states of the sample. Further, by employing a second CCD camera paired with an additional diffraction crystal simultaneous XAS/XES measurements could also be realized.[18]

The main advantage of the presented dispersive-type configuration is the lack of moving elements during the acquisition of the spectrum. The absence of motorized positioners for the crystal and detector simplifies the maintenance and operation of the setup and leaves sufficient space for implementing other instrumentations, such as advanced sample delivery systems. If a more demanding sample is studied, such as powder or solution in the form of a jet or enclosed in a cell, a small beam spot on the probed specimen provided by the polycapillary optics reduces the potential problem of sample inhomogeneity, typical of transmission mode XAS. In addition, the sample can be mounted on a motorized positioner, and by scanning along horizontal and vertical

directions, a homogenous area can be identified to exclude the problem of sample non-uniformity. The whole setup allows various sample configurations, yet it remains compact and does not require a vacuum chamber, making it easy to install and use in a lab. Helium bag can easily be applied to enhance the count rate at the photon energies below the Fe K-edge binding energy.

Due to its advantages, the dispersive von Hámos configuration is becoming fairly popular among new generations of lab-based setups. There are, however, alternative geometries, in particular Johann, which utilize x-ray spectrometers in so-called scanning mode. An example of such apparatus was described by Honkanen et al.[17] In their Johann-type spectrometer, the x-ray tube, spherically bent crystal analyzer and detector follow the Rowland circle to monochromize and focus the x-ray beam. In this configuration, only a single x-ray wavelength can be detected at a given time and the acquisition of the entire XAS spectrum requires synchronized movement of the crystal and detector. Compared to our von Hámos geometry, this approach is more advantageous for low count-rate experiments and enables the XAS signal detection in a fluorescence mode. At the same time, scanning over the whole XAS spectrum energy range makes the measurement more complicated and time-consuming. Depending on a specific experiment, one configuration would be preferred over the other. Therefore, these two spectrometer types should be thought of as a complementary tools. A more detailed overview and comparison of laboratory x-ray spectrometers could be found in a recent review article published by Zimmermann et al.[8]

To evaluate the photon counting performance of the x-ray spectrometer we conducted a systematic K-edge XAS study for 3d metals listed in Table 1. The x-ray tube voltage and current were set to 30 kV and 0.9 mA, respectively, and CCD sensors were cooled down to $-40°C$. The incident and transmitted beam spectra around the K-shell electron binding energy of each element were measured for 50 min in ambient conditions, except for the lightest Ti and Cr, where the time of data acquisition was prolonged to 100 min. The measurement times were selected to deliver counting statistics enough for the characterization of the K-edge absorption jump and energy calibration through fitting the experimental spectra to the reference ones. The obtained data were processed through Lambert-Beer law to acquire K-edge XAS spectra.

3 | RESULTS AND DISCUSSION

Due to the polychromatic source used in our setup, the signal received by the CCD camera does not consist

TABLE 1 The list of examined materials with the description of diffraction crystal and Bragg angle value used in the acquisition of K-edge XAS spectra. The last column puts together the literature sources where the reference spectra were taken from (see Results and discussion).

Element	Sample form (thickness)	K-shell binding energy E_0 [22]	Estimated detector's quantum efficiency at E_0**	Crystal used in XAS study	Bragg angle [°]	Reference spectrum
Ti	Foil (15 μm)	4966 eV	52,4%	Si(400)	66.8	[23]
Cr	Foil (4 μm)*	5989 eV	36,8%	Si(400)	49.7	[23]
Mn	Foil (5 μm)*	6539 eV	30,3%	Si(400)	44.3	[23]
Fe	Foil (5 μm)	7112 eV	25,7%	Si(440)	65.2	[24]
Co	Foil (5 μm)	7709 eV	21,4%	Si(440)	56.9	[23]
Ni	Foil (5 μm)	8333 eV	17,7%	Si(440)	50.8	[25]
Cu	Foil (10 μm)	8979 eV	14,9%	Si(440)	46.0	[26]
Zn	Foil (10 μm)	9659 eV	12,2%	Si(440)	42.0	[23]

*On 125 μm permanent polyester support.
**According to the detector's supplier brochure.

uniquely of photons diffracted by Si(110)/Si(100) crystal in the 4th order of diffraction, that is, Si(440)/Si(400), but of x-rays allowed by other diffraction orders as well. This effect is shown in Figure 2, presenting the low energy resolution spectra as a function of pixel value expressed in analog-to-digital units (ADUs) related to the electric charge released in the pixel upon absorbing a single photon. As depicted, the energy resolution of the Andor camera allows discriminating the unwanted contribution of the photons allowed by other diffraction orders, which were marked with different colors in Figure 2. In addition to the features related to Bragg-diffracted photons, each spectrum contains a peak at the position of ~150 originating from the emission of secondary x-rays of iron widely abundant in the surroundings of the spectrometer, primarily in the detector case. The resolving capability of the detector is therefore critical to filter the photons diffracted by the desired diffraction order from other unwanted radiation.

The conversion of pixel values to real photon counts requires definition of a range of pixel values $[p_0 - \Delta p, p_0]$ (here called photon energy window) regarded as resulting from absorption of a single photon of energy close to the studied K-shell binding energy (see Figure 2). Extraction of uniquely the photon counts of interest, leaving out the contribution of background x-rays which could cause distortions in the characteristic features of the XAS spectra, would thus require narrowing the energy window down to only the peak related to the relevant diffraction order, here the diffraction order of 4 (blue regions in Figure 2). It should be, however, noted that the peaks related to different diffraction orders are not symmetric and have a tail stretching toward lower ADU values (dashed line in Figure 2). Hence, narrowing the energy window to the diffraction order peak only would neglect significant
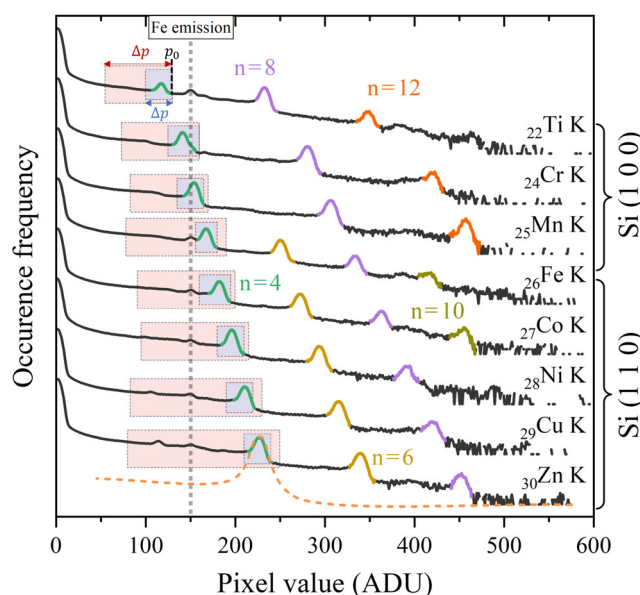

FIGURE 2 Low energy resolution spectra of the x-ray tube beam diffracted by Si crystals acquired during measurements of K-edge spectra of 3d metals. Photons diffracted by a specific diffraction order of the Si crystals are denoted with the same color. The red and blue rectangles indicate the photon energy windows used in XAS data processing. The p_0 value and Δp for both extended (red) and narrow (blue) pixel ranges are marked on the Ti K-edge histogram. Dashed line in the spectrum at the bottom outlines the actual distribution of ADU values returned by pixels illuminated with monochromatic photon beam. [Colour figure can be viewed at wileyonlinelibrary.com]

numbers of photon counts of interest and decrease the registered count rate considerably. Thus in practice, the finally selected energy window is established on the basis of a trade-off between the spectral purity and spectral statistics (red regions in Figure 2). In this work, we studied two energy windows for each measurement: one

optimized for spectral purity (termed "narrow") and another optimized for spectral intensity (termed "extended"). The narrow energy windows are tightly limited to the Si(440) and Si(400) diffraction peaks in Figure 2 to capture uniquely the photons of interest without other contributions: other diffraction orders and scattered radiation. Extending the energy window to lower pixel values increases the registered count rate as smaller fraction of pixels are discriminated. The extending thus results in the reduced point-to-point fluctuations in the measured spectra but only until a certain threshold pixel value below which the fluctuations start to rise again, mainly because of the strong contribution of the scattered radiation. The extended energy windows studied in the present work start at these threshold values, thus they can be regarded as the largest allowed.

Figure 3 presents the K-edge XAS spectra of the examined 3d metals obtained with extended (left) and narrow (right) energy window settings with the energy scale set to the position of the absorption edge (E_0) of a given element. The energy calibration was done numerically through finding the best fit of reference spectra (red lines) to the corresponding measured spectra assuming a linear pixel-to-energy conversion function and introducing photon-counting error-dependent weights of each data point and variance. The energy calibration done in this way depends mainly on the experimental precision within the energy range closest to the raising edge in the

spectrum. Fine structure observed in the K-edge XAS spectra of transition metals arises from the excitation of K-shell electron to higher unoccupied states (features on the rising edge) and the continuum (post-edge features). The spectra of Ti and Cr exhibit a relatively high statistical uncertainty regardless of the selected photon energy window. This is mainly because the binding energies of the K-shell electrons of these two specimens (given in Table 1) correspond to less energetic x-rays, which are significantly stronger attenuated by air. This effect is also shown in Figure 2 where the peak related to photons diffracted by the 4th diffraction order on the Ti low energy resolution spectrum is much smaller than the analogous peak in other spectra. The recorded manganese spectrum also showed discrepancy from the synchrotron data even beyond the statistical error. In this case, the probable reason is partial oxidation of the studied foil, which we infer from a very non-glossy look of the foil surface, characteristic of rusted foils, and from the fact that metallic manganese is most susceptible to oxidation among the metals we studied (the lowest standard oxidation potential[27–29]). As the x-ray tube anode is made of molybdenum, the detector during the Mn spectrum measurement was illuminated by the Mo $K\beta_1$ emission (19608.3 eV[22] in the 12th order of diffraction, which would correspond to about −3 eV in the acquired spectrum). This contribution is however discriminated by the energy windows applied. Results acquired for Fe, Co, Ni,
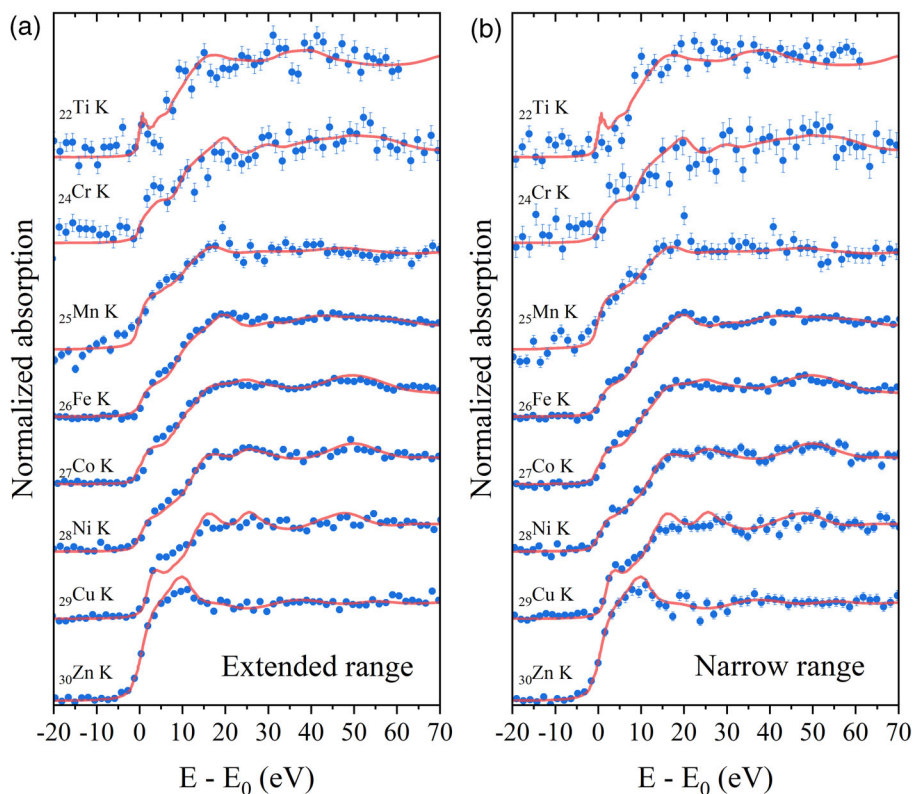

FIGURE 3 XAS K-edge spectra of examined 3d metals obtained with: (a) extended and (b) narrow photon energy window. Synchrotron reference spectra (red curves), with their publication sources listed in Table 1, were fitted to both datasets for comparison. The energy separation of spectral points is 1.5 eV in all the spectra shown. The error bars were calculated based on the counting statistical error and energy calibration error. [Colour figure can be viewed at wileyonlinelibrary.com]

Cu, and Zn show very good agreement with the reference data. However, spectra obtained with an extended photon energy window, despite their better photon counting statistics, show a noticeable deterioration of the spectral resolution leading to discrepancy from synchrotron measurements, especially in the region 0–10 eV in the Cu and Zn spectra. Narrowing the energy threshold resulted in more accurate mapping of the near-edge features, nevertheless some post-edge regions do not fully reflect the literature reports, like the structure of the Zn spectrum in the range of 15–25 eV, probably affected by the W $L\beta_1$ emission (9672.35 eV[22]) from the x-ray tube cathode. Similar interference has been observed previously with the same x-ray source[18] and cannot be filtered out using photon energy discrimination in the CCD detector because the W $L\beta_1$ photons are diffracted in the same diffraction order. Still, both series of results demonstrate the high resolution of the experimental setup and have sufficient statistics to identify the absorption edge and majority of spectral features and to ultimately estimate the registered spectral intensity.

The average registered spectral intensity of the von Hámos geometry-based laboratory x-ray spectrometer was summarized in Figure 4. The average spectral intensities $\overline{I_0}$ were calculated using the formula:

$$\overline{I_0}(E_c, d, n, p_0, \Delta p) = \frac{\dot{N}(E_c, d, n, p_0, \Delta p)}{\Delta E(E_c, d, n)} \quad (1)$$

where $\dot{N}$ is the photon count rate (in counts/second) registered by the entire CCD during the incident beam spectrum measurement and ΔE is the energy span on the CCD. ΔE depends on the arrangement for a given element which is determined by the energy of interest E_c at which the detector is centered and the used Bragg diffraction characterized by the crystal lattice spacing d and the diffraction order n.[30] In general, the setup can be arranged such that the central energy E_c is at the position of the binding energy of interest E_0 (see Table 1), however, usually the detector is shifted (and together with it is E_c) by about 10–50 eV, to cover wider range above the absorption edge in the measured XAS spectra. Similar to $\Delta E(E_c, d, n)$, the count rate $\dot{N}$ depends on the setup arrangement. In addition to that, however, $\dot{N}$ is affected by the conversion from the detector ADUs to photon counts, thus on the energy window $[p_0 - \Delta p, p_0]$. As it is shown in Figure 4, for measurements conducted with the same diffraction crystal, the average spectral intensity decreases with the increase of atomic number. Heavier elements require more energetic photons to excite the K-shell electrons, which translates to smaller Bragg angles and longer path lengths for primary x-ray beam as well as lower quantum efficiency of the CCD camera (Table 1). As presented, the setup registers the highest spectral intensity at photon energies around the Fe K absorption edge which is reflected in the high quality of the Fe K-edge XAS spectra shown in Figure 3.

4 | CONCLUSIONS

In summary, we presented the experimental operation of the von Hámos lab-based x-ray spectrometer in systematic XAS studies of various 3d metals. Important aspects regarding the selection of proper photon energy windows for XAS data processing were discussed. Performed experiments demonstrated the setup's ability for K-edge XAS measurements of transition metals in the energy range 5–10 keV. We showed that the setup allows the acquisition of high-quality XAS spectra at the laboratory scale with respectable time, which can be successfully utilized in everyday studies of various materials. Possible applications of the presented laboratory x-ray spectrometer involve studies of metallic NPs for uses in energy conversion, probing phase transitions of tunable molecular species, and characterization of catalysts to name a few. With a fairly low cost of the equipment and undemanding sample conditions, such apparatus can easily be adopted by a broader range of the scientific community extending the availability of XAS beyond synchrotron facilities.
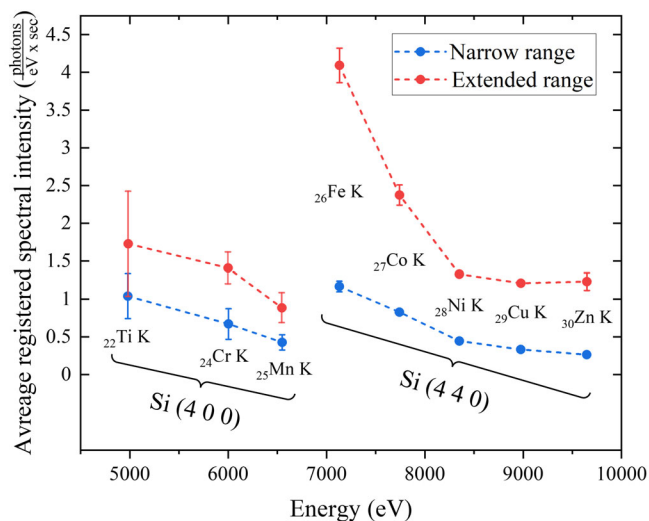

FIGURE 4 Photon counting performance of the presented XAS setup. Data obtained with narrow and extended photon energy windows are denoted with blue and red points, respectively. The error bars do not reach out the data point markers for Ni and Cu for the extended and Co, Ni, Cu and Zn for the narrow photon energy window. [Colour figure can be viewed at wileyonlinelibrary.com]

DATA AVAILABILITY STATEMENT

The data that support the findings of this study are available from the corresponding author upon reasonable request.

ORCID

Rafał Fanselow https://orcid.org/0000-0002-0939-4590
Wojciech Błachucki https://orcid.org/0000-0003-4457-2345

REFERENCES

[1] T. Guo, *Laser Photonics Rev.* **2009**, *3*(6), 591.

[2] A. Wach, J. Sá, J. Szlachetko, *J. Synchrotron Radiat.* **2020**, *27*, 689.

[3] L. Zhang, D. Sun, J. Kang, H. T. Wang, S. H. Hsieh, W. F. Pong, H. A. Bechtel, J. Feng, L. W. Wang, E. J. Cairns, J. Guo, *Nano Lett.* **2018**, *18*(7), 4506.

[4] R. S. K. Lam, R. A. Metzler, P. U. P. A. Gilbert, E. Beniash, *ACS Chem. Biol.* **2012**, *7*(3), 476.

[5] J. Czapla-Masztafiak, A. Kubas, Y. Kayser, D. L. A. Fernandes, W. M. Kwiatek, E. Lipiec, G. B. Deacon, K. al-Jorani, B. R. Wood, J. Szlachetko, J. Sá, *J. Inorg. Biochem.* **2018**, *187*(July), 56.

[6] J. Lin, E. Wiens, N. Chen, M. J. Nilges, W. Chen, Y. Pan, *Environ. Sci. Technol.* **2022**, *56*, 5563.

[7] R. Bès, T. Ahopelto, A. P. Honkanen, S. Huotari, G. Leinders, J. Pakarinen, K. Kvashnina, *J. Nucl. Mater.* **2018**, *507*, 50.

[8] P. Zimmermann, S. Peredkov, P. M. Abdala, S. DeBeer, M. Tromp, C. Müller, J. A. van Bokhoven, *Coord. Chem. Rev.* **2020**, *423*, 213466.

[9] W. Malzer, C. Schlesiger, B. Kanngießer, *Spectrochim. Acta Part B At. Spectrosc.* **2020**, *177*(November), 2021.

[10] P. Lecante, J. Jaud, A. Mosset, J. Galy, A. Burian, *Rev. Sci. Instrum.* **1994**, *65*(4), 845.

[11] K. Tohji, Y. Udagawa, *Jpn. J. Appl. Phys. Part 1 Regul. Pap. Short Notes* **1983**, *22*(5), 882.

[12] A. Williams, *Rev. Sci. Instrum.* **1983**, *54*(2), 193.

[13] J. Hoszowska, J. C. Dousse, J. Kern, C. Rhême, *Nucl. Instrum. Methods Phys. Res. Sect. A Accel. Spectrom. Detect. Assoc. Equip.* **1996**, *376*(1), 129.

[14] G. T. Seidler, D. R. Mortensen, A. J. Remesnik, J. I. Pacold, N. A. Ball, N. Barry, M. Styczinski, O. R. Hoidn, *Rev. Sci. Instrum.* **2014**, *85*(11), 113906.

[15] Z. Németh, J. Szlachetko, É. G. Bajnóczi, G. Vankó, *Rev. Sci. Instrum.* **2016**, *87*(10), 103105.

[16] C. Schlesiger, L. Anklamm, H. Stiel, W. Malzer, B. Kanngießer, *J. Anal. At. Spectrom.* **2015**, *30*(5), 1080.

[17] A. P. Honkanen, S. Ollikkala, T. Ahopelto, A. J. Kallio, M. Blomberg, S. Huotari, *Rev. Sci. Instrum.* **2019**, *90*(3), 033107. https://doi.org/10.1063/1.5084049

[18] W. Błachucki, J. Czapla-Masztafiak, J. Sá, J. Szlachetko, *J. Anal. At. Spectrom.* **2019**, *34*(7), 1409.

[19] W. Stańczyk, J. Czapla-Masztafiak, *Nucl. Instrum. Methods Phys. Res. Sect. B Beam Interact. Mater. Atoms* **2021**, *497*(June 2020), 65.

[20] R. Fanselow, A. Wach, W. Błachucki, J. Szlachetko, *Spectrochim. Acta Part B At. Spectrosc.* **2021**, *189*(September), 2022.

[21] J. Szlachetko, M. Nachtegaal, E. de Boni, M. Willimann, O. Safonova, J. Sa, G. Smolentsev, M. Szlachetko, J. A. van Bokhoven, J. C. Dousse, J. Hoszowska, Y. Kayser, P. Jagodzinski, A. Bergamaschi, B. Schmitt, C. David, A. Lücke, *Rev. Sci. Instrum.* **2012**, *83*(10), 103105.

[22] A. C. Thompson, D. Vaughan, *X-Ray Data Booklet*, Lawrence Berkeley National Laboratory, Berkeley, **2009**, p. 176.

[23] EXAFS_Materials, **2007**, *925*. exafsmaterials.com/ReferenceSpectra.html.

[24] Z. Guo, L. L. Henry, V. Palshin, E. J. Podlaha, *J. Mater. Chem.* **2006**, *50*, 1772.

[25] D. Pan, J. K. Jian, A. Ablat, J. Li, Y. F. Sun, R. Wu, *J. Appl. Phys.* **2012**, *112*(5), 053911. https://doi.org/10.1063/1.4749408

[26] G. Silversmit, H. Poelman, V. Balcaen, P. M. Heynderickx, M. Olea, S. Nikitenko, W. Bras, P. F. Smet, D. Poelman, R. de Gryse, M. F. Reniers, G. B. Marin, *J. Phys. Chem. Solids* **2009**, *70*(9), 1274.

[27] W. M. Haynes Ed., *CRC Handbook of Chemistry and Physics*, 95th ed., CRC Press, Boca Raton **2014**. https://doi.org/10.1201/b17118

[28] A. J. Bard, R. Parsons, J. Jordan, *Standard Potentials in Aqueous Solution*, 1st ed., Routledge, New York, **1985**. https://doi.org/10.1201/9780203738764

[29] P. W. Atkins, *Physical Chemistry*, 6th ed., W. H. Freeman & Co., New York, ISBN 9780716734659 **1997**.

[30] Y. Kayser, '*Synchrotron radiation based high–resolution grazing emission X–ray fluorescence*', PhD thesis, chapter: Von Hámos spectrometer, University of Fribourg (Switzerland), **2011**.